Ab initio and experimental oxygen ion conductivities in Sm-Zr and Gd-Zr co-doped ceria

Julius Koettgen[a,b,c,d,*], Steffen Grieshammer[a,b,e], Gerald Dück[a], Gregor Ulbrich[f], Martin Lerch[f] and Manfred Martin[a,b,e,g]

[a]Institute of Physical Chemistry, RWTH Aachen University, Landoltweg 2, 52056 Aachen, Germany
[b]JARA-HPC, Forschungszentrum Jülich and RWTH Aachen University, Germany
[c]Materials Sciences Division, Lawrence Berkeley National Laboratory, Berkeley, California 94720, United States
[d]Department of Materials Science and Engineering, University of California, Berkeley, California 94720, United States
[e]Helmholtz-Institut Münster (IEK-12), Forschungszentrum Jülich GmbH, Corrensstr. 46, 48149 Münster, Germany
[f]Institute of Chemistry, Technical University of Berlin, Straße des 17. Juni 124, 10623 Berlin, Germany
[g]JARA-Energy, Forschungszentrum Jülich and RWTH Aachen University, Germany

ARTICLE INFO

Keywords:
Oxides;
Defects;
Doping;
Ceria

Abstract

The oxygen ion conductivities of Sm doped ceria and Gd doped ceria are the highest for a rare-earth doped cerium oxide, which can be applied in solid oxide fuel cells (SOFC), high-temperature electrolysis with solid oxide electrolysis cells (SOEC), and high-temperature batteries. At the same time, zirconium oxide is a common impurity that has been shown to reduce the ionic conductivity in this type of doped ceria material. Doping with zirconia does not create additional oxygen vacancies and the conductivity is only influenced by the additional interactions between the Zr ions and either the rare-earth dopants or the oxygen vacancies. In this work, ceria co-doped with Sm-Zr and Gd-Zr is investigated using impedance spectroscopy experiments as well as density functional theory calculations and Kinetic Monte Carlo simulations. Co-doping Sm-doped and Gd-doped ceria with Zr decreases the conductivity significantly in experiments and simulations. The strong influence on the conductivity is due to the effective trapping of the oxygen vacancies by the zirconium ions.

This is the accepted manuscript of an article published in Solid State Ionics:
J. Koettgen, S. Grieshammer, G. Dück, G. Ulbrich, M. Lerch, M. Martin, Ab initio and experimental oxygen ion conductivities in Sm-Zr and Gd-Zr co-doped ceria, Solid State Ionics, 355 (2020) 115422.
DOI: 10.1016/j.ssi.2020.115422
http://dx.doi.org/10.1016/j.ssi.2020.115422

1. Introduction

Solid solutions of ceria (CeO_2) and rare-earth oxides (RE_2O_3) are known for their high oxygen ion conductivity. As a result, rare-earth doped ceria can be used as electrolyte in solid oxide fuel cells, electrolyzer cells, and high-temperature batteries.[1] The high ionic conductivity can be attributed to the creation of oxygen vacancies $V_O^{\bullet\bullet}$ by doping, as shown in Eq. 1 in Kröger-Vink notation.[2]

$$RE_2O_3 \longrightarrow 2\,RE'_{Ce} + 3\,O_O^{\times} + V_O^{\bullet\bullet} \tag{1}$$

Defect interactions cause increased migration barriers for oxygen vacancy jumps around dopants (blocking). Blocking appears at configurations where the two adjacent Ce cations along the migration pathway of the oxygen (migration edge, Fig. 1) are partly or fully substituted by large rare-earth dopants.[3, 4, 5] Additionally, the association between dopants and oxygen vacancies increases migration barriers for oxygen jumps away from dopants (trapping) and decreases migration barriers for oxygen jumps towards dopants.[3, 4]

Sm and Gd doped ceria show the highest ionic conductivities in experiments.[6, 7, 8, 9, 10, 11, 12, 13, 14, 15, 16, 17, 18, 19, 20, 21, 22] In our previous work, we investigated the influence of blocking and trapping on the ionic conductivity

julius.koettgen@rwth-aachen.de (J. Koettgen); martin@rwth-aachen.de (M. Martin)
ORCID(s): 0000-0002-8260-4793 (J. Koettgen); 0000-0001-9046-050X (M. Martin)

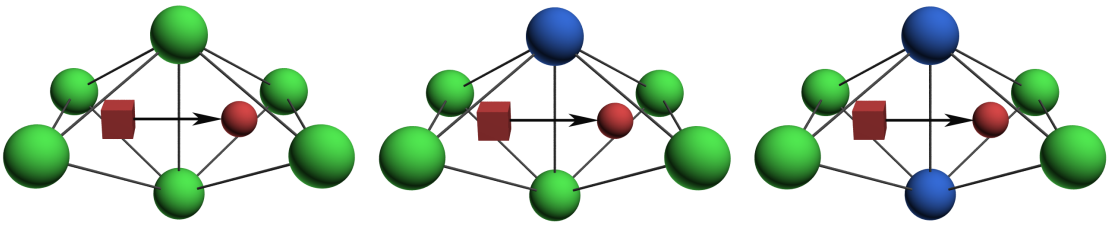

Figure 1: Possible migration edge configurations in samarium doped ceria. Ce-Ce edge (left), Ce-Sm edge (middle) and Sm-Sm edge (right). Cerium ions (green), samarium ions (blue), oxygen ions (red spheres) and oxygen vacancies (red boxes).[4] - Reproduced by permission of the PCCP Owner Societies

using Kinetic Monte Carlo (KMC) simulations with a migration energy model based on density functional theory (DFT) calculations.[3] We could show that Sm and Gd dopants have the best combination between weak blocking and weak trapping, and our simulation results were in good agreement with experimental data. In a further step, we extended our simulation model to co-doping with zirconium for the case of Y doped ceria.[23] In applications, Zr doping is used to increase the performance in the production of solar fuels as well as in catalytic processes such as in automotive three-way catalysts due to the increased oxygen storage capacity (OSC).[24, 25, 26, 27, 28] However, in these applications, much higher Zr contents are used to improve the reducibility of ceria materials rather than their ionic conductivity behavior. Additionally, Zr is a common impurity in ceria due to impure raw materials or cation diffusion from adjacent phases in solid electrochemical cells, explaining the importance of the investigation of co-doped ceria.[29, 30, 31] Doping ceria with zirconia is of particular interest since zirconium has the same valence as the host cation ceria. Therefore, doping with zirconia does not create additional oxygen vacancies and the conductivity is only influenced by the additional association or blocking of the oxygen vacancies as discussed in theoretical literature.[32, 33, 34, 35] Our simulations,[23] as well as previous experimental studies in Y doped ceria,[30] show that doping with Zr decreases the conductivity.

In this work, we investigate the influence of Zr co-doping on the ionic conductivity in Sm and Gd doped ceria (e.g., $Ce_{1-x-y}Zr_ySm_xO_{2-x/2}$) by experimental and computational methods. Simulations are based on DFT and KMC methods exploiting our previously described approach.[3, 23] For this purpose, we predict ionic conductivities using Kinetic Monte Carlo (KMC) simulations with a migration energy model based on density functional theory (DFT) calculations. Experiments are performed on polycrystalline samples and quasi single crystalline samples (agglomerates of large grains) using impedance spectroscopy.

The paper is organized as follows: In section 2, details concerning the prepared samples and the experimental setup are described. In section 3, details of the calculations are given. In section 4, we present our experimental and theoretical results for the ionic conductivity in co-doped ceria. In section 5, we give a short summary.

2. Experimental details

Single crystals with the compositions $Ce_{0.889}Zr_{0.006}Gd_{0.105}O_{1.9475}$ and $Ce_{0.887}Zr_{0.043}Sm_{0.070}O_{1.965}$ were synthesized by skull-melting.[36] Powders of the binary oxides were carefully mixed in the respective ratios (ZrO_2 99.91% purity, Surface Net, Rheine, Germany, Sm_2O_3, Gd_2O_3 and CeO_2 99.9% purity, Chempur, Karlsruhe, Germany, ignition material: Zr 99.6% purity, Haines & Maassen, Bonn, Germany). Skull-melting is a quasi crucible-free high frequency (HF) process in which the material is kept in a water-cooled crucible. The melt is surrounded by a thin ceramic layer of unmolten material protecting it from impurities. Chemical compositions were determined via wavelength-dispersive X-ray spectroscopy (WDS) with an electron beam micro probe (Cameca Camebax Microbeam, Gennevilliers, France). During skull-melting, an agglomerate of single crystals with very large grain sizes (about 500 μm) is grown. X-ray diffraction was performed to identify the crystallographic phases. For this purpose, the agglomerates of single crystals were ground in a mortar and the powders were investigated using a "PANalytical X'Pert PRO MPD" diffractometer equipped with a "PIXcel" detector using nickel-filtered Cu-Kα radiation. Additional investigations were performed on a "Rigaku SmartLab 3 kW" system equipped with a Johansson-type Ge monochromator using Cu-Kα1 radiation. A 2θ range between at least 20° and 80° and a step size of 0.05° was applied (see supporting information). The agglomerates of single crystals were also checked by Laue backscattering (tungsten radiation, photosensitive image plates, STOE & Cie GmbH, Darmstadt, Germany) and Inductively coupled plasma

optical emission spectroscopy (OPTIMA 4300 DV, Perkin-Elmer).[36] Polycrystalline samples were prepared according to an earlier work[37] by dissolving cerium (III) nitrate hexahydrate (99.9%, Chempur), rare-earth nitrate hydrate ($RE(NO_3)_z \cdot x\,H_2O$, 99.9 %, with $z = 3$ for Sm: Sigma-Aldrich, Gd: Strem Chemicals or $z = 4$ for Zr: Alfa Aesar) and citric acid (VWR International, 2.5 equivalents) in water. The water content in the nitrate hydrates was determined and verified by dehydration and gravimetric analysis. The sol-gel transformation occurred during the mixing for several hours at 50 °C. At 350 °C, the produced foam was dried for three hours and subsequently calcined for four hours at 1000 °C. The calcined powder was dry milled in a planetary mill, uniaxially pressed to disks (10 mm in diameter and 2 mm thick) and sintered in air at 1400 °C for 24 hours. The composition was successfully verified using X-ray diffraction (Theta-Theta diffractometer, STOE, Darmstadt, Germany) and Rietveld refinement, energy-dispersive X-ray spectroscopy measurements (Oxford INCA, Oxford Instruments, Abingdon, UK), wavelength-dispersive X-ray spectroscopy measurements (Jeol JXA-8530F, JEOL USA Inc., Peabody USA).[38, 3] Significant efforts have been performed to minimize the error (about 0.2 atom-%) of the determined stoichiometry, which is significant for the Zr content in the $Ce_{0.889}Zr_{0.006}Gd_{0.105}O_{1.9475}$ composition. Density measurements of the polycrystalline samples according to the Archimedes method gave high densities around 95% of the theoretical value. Scanning electron microscope measurements (LEO 1450VP, Carl Zeiss, Oberkochen, Germany) of samples etched in 32 % HCl at room temperature for five minutes show that grain sizes are about 1 μm for the polycrystalline doped ceria, for an example see supporting information.

For impedance measurements, electrodes made of platinum paste were used and connected with platinum wire. The conductivity experiments were performed in air and at temperatures between room temperature and 700°C after an equilibration time of 3 hours. Impedance spectroscopy measurements were realized using a two-point geometry (Solartron 1260) with frequencies between 10^7 and $7 \cdot 10^{-2}$ Hz. In the impedance spectra, the bulk and grain boundary semicircles were identified according to literature.[39] The depressed bulk semicircles in the complex impedance plot were analyzed using an equivalent circuit composed of an RQ-element with the constant phase element Q. The ionic conductivity was calculated according to $\sigma = \frac{d}{AR}$ with the sample thickness d and the area A yielding the bulk conductivity σ_{bulk} and the macroscopic grain boundary conductivity σ_{gb}. The error of the ionic conductivity is about 2%.

3. Computational details

Quantum mechanical calculations were executed according to earlier works[4, 29, 40, 3, 41, 37] using the Vienna Ab initio Simulation Package (VASP)[42, 43] calculating geometric parameters and energies at zero temperature. All *ab initio* calculations were performed within the scope of the density functional theory (DFT) using the Generalized Gradient Approximation (GGA) according to Perdew, Burke and Ernzerhof (PBE)[44, 45] and the projector augmented-wave method (PAW).[46] An energy cut-off of 500 eV was chosen for the plane waves. Supercells consisting of 8 unit cells (a multiplication of $2 \times 2 \times 2$ unit cells in each dimension) and 27 unit cells ($3 \times 3 \times 3$) were employed. Monkhorst-Pack k-point meshes of $2 \times 2 \times 2$ and $1 \times 1 \times 1$ were applied, respectively. The $5s^2 5p^6 6s^2 5d^1 4f^1$ electrons of the cerium atoms were treated as valence electrons. Similarly, the $5s^2 5p^6 6s^2 5d^1$ electrons of the samarium atoms, the $5p^6 6s^2 5d^1$ electrons of the gadolinium atoms, and the $2s^2 2p^4$ electrons of the oxygen atoms were treated as valence electrons. To account for the localization of strongly correlated f-electrons, a Hubbard U parameter was introduced by the rotational invariant approach.[47] The repulsion parameter of $U = 5$ eV for the 4f-orbitals of cerium was chosen according to literature.[48, 49, 50, 25, 51, 52, 53, 54, 55] The total number of electrons in the cell was adjusted for all defective cells to reproduce the actual charge state of the defects, e.g. $\left(Ce_{108}O_{215}\right)^{2+}$ for a $3 \times 3 \times 3$ supercell containing one oxygen vacancy. Charged cells are calculated assuming a neutralizing background charge, which is a valid approach as shown in literature.[56, 57, 58, 59]

The convergence parameters for electronic and ionic relaxation were set to at least 10^{-5} eV and 10^{-2} eV/Å, respectively, to guarantee a sufficient accuracy of the calculated forces. A lattice constant of 5.49 Å was calculated for defect-free ceria using the Birch-Murnaghan equation of state. This parameter is larger than the experimental lattice parameter due to the chosen set of parameters,[60, 61, 62, 40] and applied for all calculations as performed in literature.[63, 64, 65] The lattice parameter for $Ce_{0.9}Zr_{0.1}O_2$ (5.456 Å) is given by the calculated lattice parameters of CeO_2 (5.49 Å) and ZrO_2 (5.15 Å) according to Vegard's law.[23] The internal atomic positions in the cell were relaxed (changed to minimize the energy of the cell) without changing the lattice parameter for all calculations. The transition states and the minimum energy pathways were investigated using the nudged elastic band (NEB)[66, 67, 68] and climbing image NEB methods[69]. The ionic configuration for the saddle point configuration ('image') was inter-

polated from the initial and final state of the migration process. Tests with more than one intermediate image between the initial and final configuration of the migration showed no differences in the migration energies. Association and migration energies strongly depend on the finite supercell size due to the interactions of the defects with their image in other cells and, therefore, the dipole interaction is corrected according to Makov and Payne.[70]

For the migration energy model, migration energies for the migration edge (Fig. 1) are combined with pair interactions to predict the barrier for every possible ionic configuration including multiple dopants and oxygen vacancies around the jumping oxygen vacancy. The simulated ionic conductivities for Sm and Gd doped ceria are in agreement with experiments.[3]

For co-doped ceria, migration energies depend not only on the individual migration edges (e.g., Ce-Ce, Ce-Sm, Sm-Sm, Ce-Zr and Zr-Zr) and association energies but also on mixed migration edge energies (Sm-Zr). Only few simulations of co-doped ceria were performed in literature before.[71] Thus, we are confident that our proposed migration energy model is a significant improvement of earlier works.[23]

Ionic conductivities were simulated by means of the Kinetic Monte Carlo simulations using the in-house code iCon.[72] In literature, the oxygen ion conductivity in ceria was calculated using analytical models[73, 74] and Kinetic Monte Carlo (KMC) simulations,[75, 76, 77, 78, 79, 71, 55, 80, 4, 81] which we significantly improved in our earlier works.[4, 3, 23] A $14 \times 14 \times 14$ supercell with 32928 ions (Ce, RE, O) and vacancies, periodic boundary conditions and a random cation distribution were used. An electric field strength equal to $0.1\frac{2k_BT}{ql}$ with the oxygen ion charge q and the jump distance l was used, which had no influence on the thermodynamic equilibrium according to an earlier work.[4, 82] An attempt frequency of $3.2 \cdot 10^{12}$ Hz for the oxygen vacancy jump was chosen in agreement with our earlier work.[23, 29] Simulations were performed with 150 MCSP for compositions without zirconium doping and up to $2 \cdot 10^4$ for zirconium co-doped compositions. The reason for the higher MCSP in the latter case is the strong trapping of the vacancies by the zirconium dopants. Prior to the evaluation of the conductivity, the anion sub-lattice was equilibrated with 10% of the steps. All simulations were repeated ten times with different random cation distributions.

4. Results and discussion

4.1. Experiments

Impedance spectroscopy measurements reveal three semicircles, which can be attributed to the bulk , with a capacitance of about $5 \cdot 10^{-11}$ F, the grain boundary, with a capacitance of about $5 \cdot 10^{-9}$ F, and the electrode with an even larger capacitance according to literature.[39, 83, 14] Bulk, grain boundary and electrode semicircles of Sm-Zr and Gd-Zr doped ceria can only be observed in a limited temperature range due to the limited frequency range. For the agglomerate of single crystals, the semicircle for the grain boundary is strongly diminished due to the small number of grain boundaries (see supporting information).

Figure 2 shows the ionic conductivity for the bulk σ_{bulk} of Sm-Zr doped ceria. The curves show a slight curvature as described in literature.[84, 9, 10, 18, 85, 6, 86, 13] Doping with Zr decreases the conductivity significantly and increases the activation enthalpy. The change of the Sm dopant fraction is below 1 % which can explain less than 30% change in conductivity,[3] As the measured conductivities decrease by more than 95 %, co-doping with Zr is the main reason for the decreased conductivities. It is apparent that the bulk ionic conductivity of the polycrystalline sample and the quasi single crystal with similar composition are not the same. On the one hand, this could be due to unidentified deviations in the compositions as small changes of the Zr content have a large impact on the ionic conductivity as discussed above. On the other hand, this could be due to uncertainties in the decomposition of the semicircles. Since the influence of grain boundaries is minimized in the case of the quasi singe crystals, we consider these as a reference.

For the polycrystalline samples, the macroscopic grain boundary conductivity σ_{gb} is significantly lower than the bulk conductivity in accordance with literature. The grain boundary conductivity (Fig. 3) also decreases with Zr while the activation enthalpy increases. An exception is the single crystal agglomerate, which has an exceptionally high macroscopic grain boundary conductivity compared to the polycrystalline samples with similar composition. In the literature such microstructural variations are taken into account by calculating the specific or microscopic grain boundary conductivity[87, 88] using the serial brick layer model.[89, 90] While the macroscopic grain boundary conductivity σ_{gb} is independent of the sample dimensions according to $\sigma_{\text{gb}} = \frac{d}{AR_{\text{gb}}}$ with the sample thickness d and the area A, the microscopic grain boundary conductivity is micro-structure-independent according to $\sigma_{\text{gb, mic}} = \frac{\delta}{D}\frac{d}{AR_{\text{gb}}}$ with the grain boundary thickness δ and the grain size D. In literature, it is often assumed that the dielectric constant of the grain boundaries is approximately equal to that in the bulk and the ratio $\delta/D = C_{\text{bulk}}/C_{\text{gb}}$ is calcu-

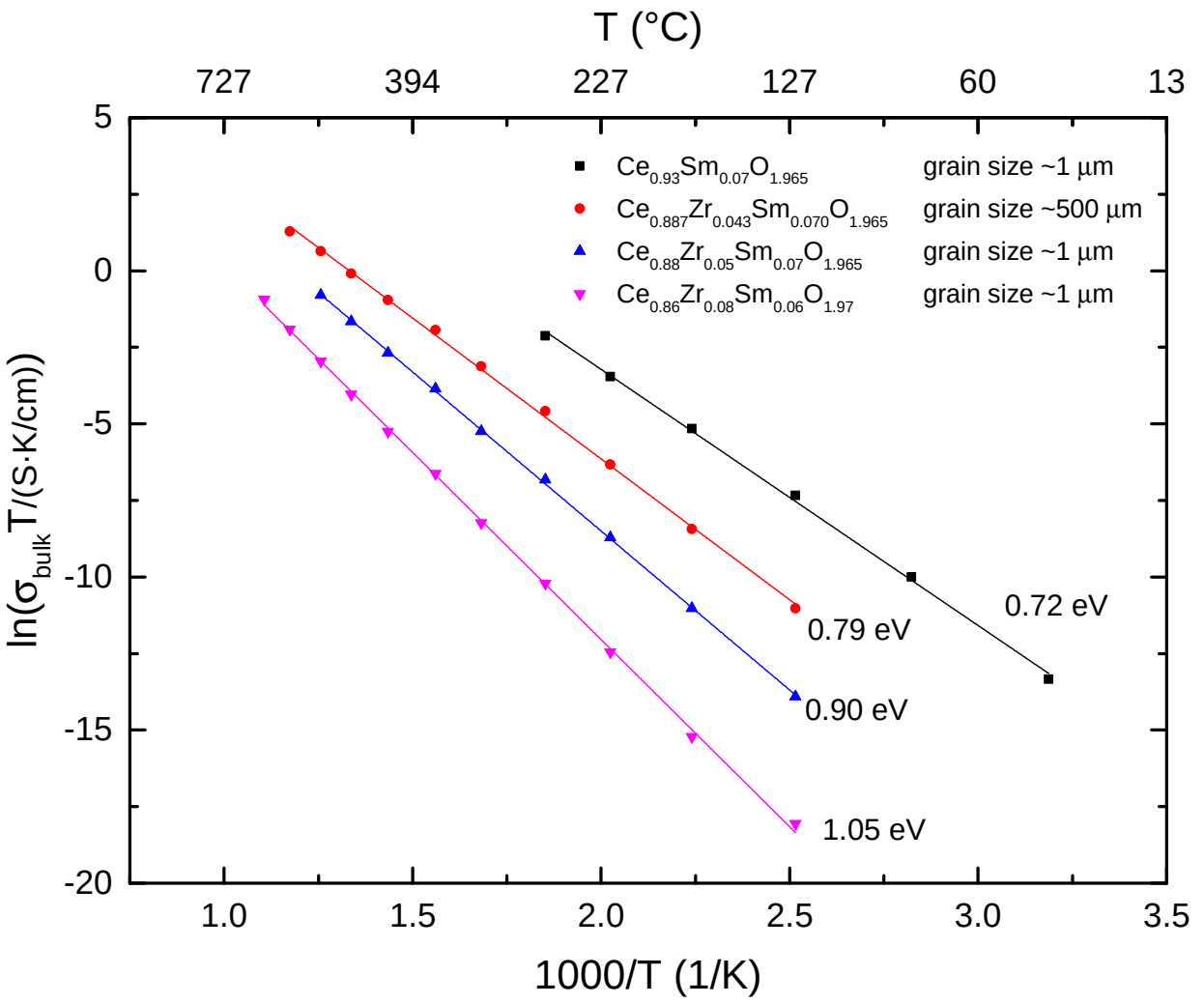

Figure 2: Ionic conductivity for the bulk of Sm doped and Sm-Zr doped ceria according to impedance experiments. Both, polycrystalline samples and an agglomerate of single crystals are investigated. Doping with Zr decreases the conductivity.

lated using the capacities of the bulk and grain boundary. In this work, the differences in grain size D are far greater than any differences in the grain boundary thickness δ. As a result, the microscopic grain boundary conductivity ratio $\sigma_{\text{gb, mic}}\left(Ce_{0.887}Zr_{0.043}Sm_{0.070}O_{1.965}\right)/\sigma_{\text{gb, mic}}\left(Ce_{0.93}Sm_{0.07}O_{1.965}\right)$ is two orders of magnitudes smaller than the macroscopic grain boundary conductivity ratio $\sigma_{\text{gb}}\left(Ce_{0.887}Zr_{0.043}Sm_{0.070}O_{1.965}\right)/\sigma_{\text{gb}}\left(Ce_{0.93}Sm_{0.07}O_{1.965}\right)$. This easily explains the high macroscopic grain boundary conductivity of $Ce_{0.887}Zr_{0.043}Sm_{0.070}O_{1.965}$ in Fig. 3. The microscopic grain boundary conductivities of $Ce_{0.887}Zr_{0.043}Sm_{0.070}O_{1.965}$ are similar to those of $Ce_{0.88}Zr_{0.05}Sm_{0.07}O_{1.965}$.

The total conductivity (Eq. 2) is again very similar to the grain boundary conductivity and deviates only at high temperatures. Due to the influence of the bulk contribution, the activation enthalpies are slightly lower as well.

$$\sigma_{\text{total}} = \frac{\sigma_{\text{bulk}} \cdot \sigma_{\text{gb}}}{\sigma_{\text{bulk}} + \sigma_{\text{gb}}}. \tag{2}$$

Ionic conductivities for the bulk, grain boundary and total ionic conductivity of Gd-Zr doped ceria are shown in Fig. 4. Compared to Sm-Zr co-doped ceria, co-doping with Zr decreases the conductivity of Gd doped ceria more pronounced.

In conclusion, the ionic conductivity decreases with increasing Zr fraction according to impedance experiments in this work and literature.[30] Therefore, Zr impurities, have to be minimized for applications demanding a high ionic

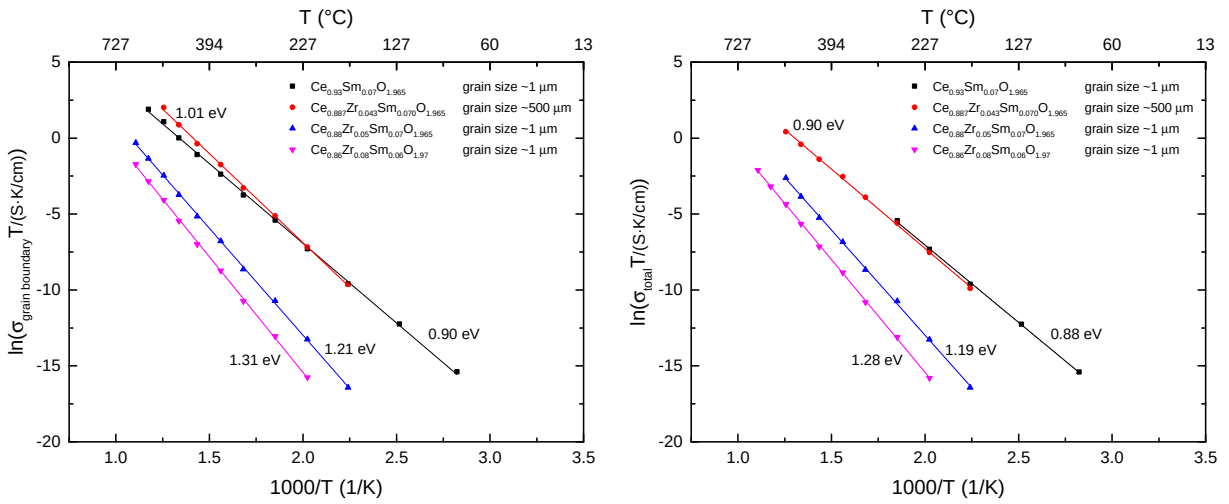

Figure 3: Macroscopic grain boundary (left) and total (right) conductivity of Sm-Zr doped ceria according to impedance experiments. Both, polycrystalline samples and an agglomerate of single crystals are investigated.

conductivity. The decrease is more pronounced in Gd than in Sm co-doped ceria.

4.2. Kinetic Monte Carlo Simulations

In the Kinetic Monte Carlo simulations an energy model from an earlier publication was applied including pair interactions of defects and migration edge energies.[23, 3] The applied pair energies and edge energies are shown in Fig. 5. As the Zr^{4+} ion is considerably smaller than the Ce^{4+} ion, doping with zirconium leads to a decrease of the lattice parameter. This decrease of the lattice parameter results in a stronger interaction between defects and an increase of the migration barriers.[23, 91] To include this effect, energies were calculated for various lattice parameters (see supporting information) and the energy model was parametrized depending on the Zr fraction as described in our earlier publication.[23]

The simulated conductivities as given in Fig. 6 show the same trends as the experimental data. Sm-doping leads to a higher conductivity than Gd-doping while co-doping with zirconium decreases the conductivity in both cases. The change in conductivity from $Ce_{0.9}Gd_{0.1}O_{1.95}$ to $Ce_{0.889}Zr_{0.006}Gd_{0.105}O_{1.9475}$ in the simulations is less pronounced than in the experiment. This is presumably due to deviations in the experimentally obtained stoichiometry on the one hand and limitations of the energy model used in the simulations on the other hand.

In summary, the doping with zirconium has three effects:[23] 1. The migration barrier is reduced when Zr ions are located at the migration edge. 2. The vacancies are strongly trapped by Zr ions. 3. Increasing the zirconium content increases defect interactions and all migration barriers through the decrease of the lattice parameter. The dominating effect here is the trapping of the vacancies at the zirconium ions that effectively lowers the average vacancy mobility.[23]

5. Conclusion

The oxygen ion conductivity of co-doped Sm-Zr and Gd-Zr ceria were investigated. Doping ceria with Zr decreases the conductivity significantly. The decrease is more pronounced in Gd than in Sm co-doped ceria. Comparison between polycrystalline samples and agglomerates of single crystals show an increase in the macroscopic grain boundary conductivity with increasing grain size.

The Kinetic Monte Carlo simulations show the same trend for the decrease of the ionic conductivity due to Zr doping. However, in this case the effect on Sm-doped ceria is more pronounced. The strong influence on the conductivity is due to the effective trapping of the oxygen vacancies by the zirconium ions. The Kinetic Monte Carlo simulations are qualitatively in agreement with the experiments. Moreover, the comparison of experimental samples shows that accurate separation of bulk and grain boundary semicircles in polycrystalline samples as well as determination of exact stoichiometry remains a difficult task and can influence the results significantly.

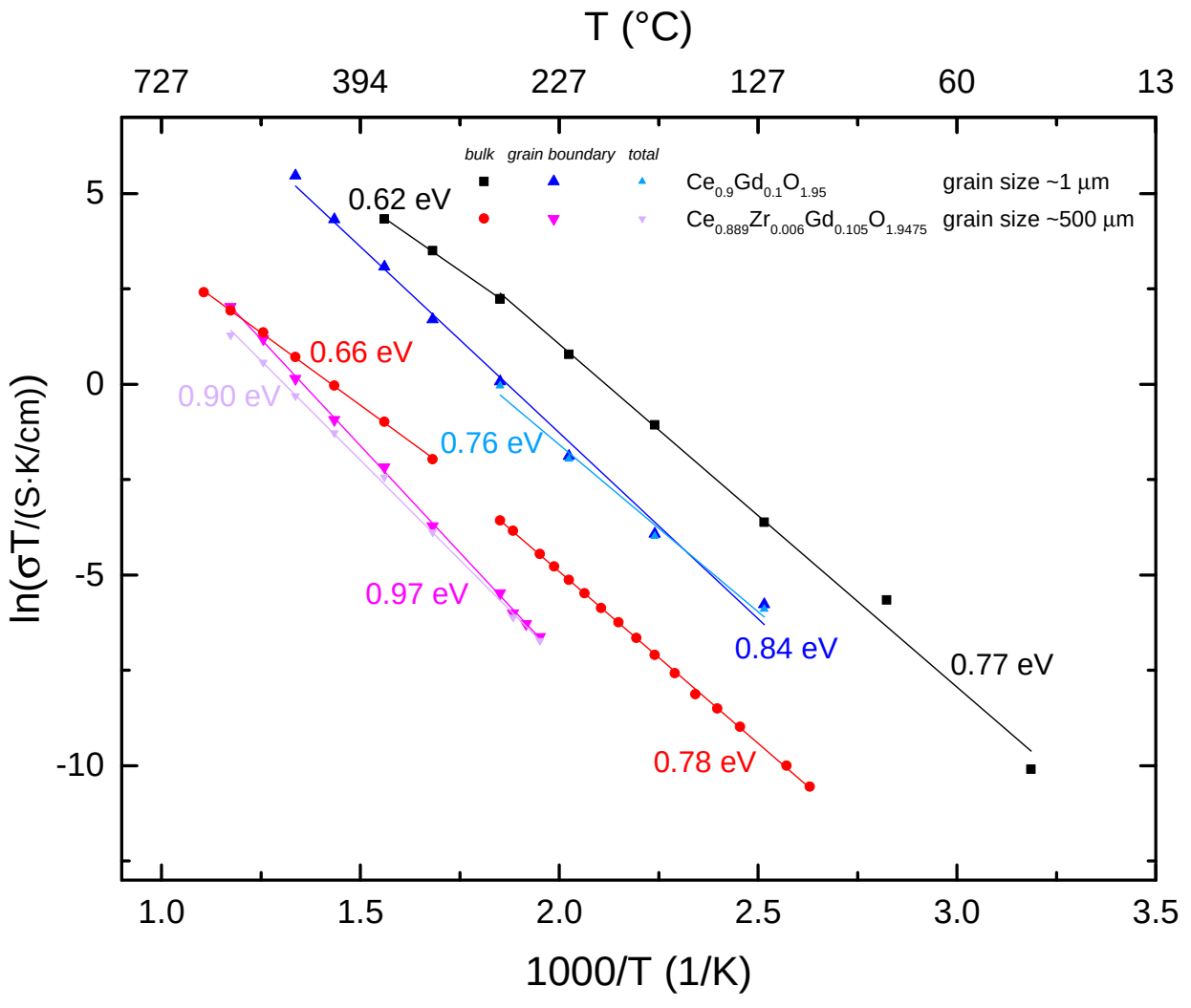

Figure 4: Ionic conductivity for the bulk, grain boundary and total domain of Gd-Zr doped ceria according to impedance experiments. Both, polycrystalline samples and an agglomerate of single crystals are investigated.

Acknowledgements

The authors gratefully acknowledge the computing time granted by the JARA-HPC Vergabegremium and provided on the JARA-HPC Partition part of the supercomputer JURECA at Forschungszentrum Jülich.[92] Simulations were performed with computing resources granted by RWTH Aachen University under project rwth0336. The authors gratefully acknowledge the computing time granted by the JARA-HPC Vergabegremium and provided on the JARA-HPC Partition part of the supercomputer CLAIX at RWTH Aachen University. Research supported by the U.S. Department of Energy, Office of Science, Basic Energy Sciences, Materials Sciences and Engineering Division under Contract No. DE-AC02-05-CH11231.

References

[1] B. C. H. Steele and A. Heinzel, *Nature*, 2001, **414**, 345–352.
[2] M. Mogensen, *Solid State Ionics*, 2000, **129**, 63–94.
[3] J. Koettgen, S. Grieshammer, P. Hein, B. O. H. Grope, M. Nakayama and M. Martin, *Physical Chemistry Chemical Physics*, 2018, **20**, 14291–14321.
[4] S. Grieshammer, B. O. H. Grope, J. Koettgen and M. Martin, *Physical Chemistry Chemical Physics*, 2014, **16**, 9974.
[5] J. Koettgen, G. Dück and M. Martin, *Journal of Physics: Condensed Matter*, 2020, **32**, 265402.

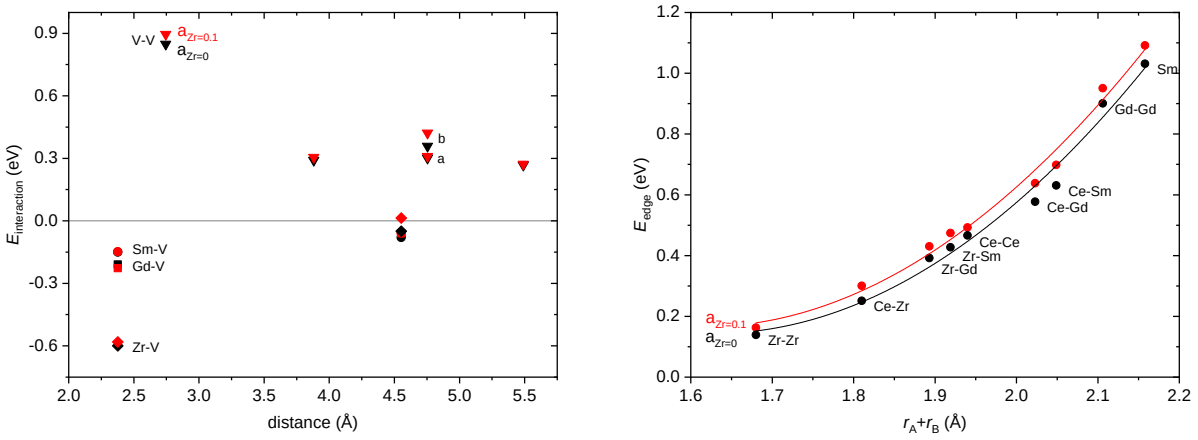

Figure 5: Pair interaction energies of an oxygen vacancy with another vacancy or dopant depending on the defect distance (left). At 4.8 Å two distinct vacancy-vacancy interactions exist with (b) and without (a) a cerium ion between the vacancies. Migration energies for the specific edge configurations depending on the sum of the cation radii (right). Lines on the right represent a parabolic fit of the energies. Energies are given for the lattice parameter of pure ceria (black) and the lattice parameter corresponding to a Zr-content of 10% (red). See ref.[23] for more details.

[6] Z. Zhan, T.-L. Wen, H. Tu and Z.-Y. Lu, *Journal of The Electrochemical Society*, 2001, **148**, A427.
[7] R. Sanghavi, R. Devanathan, M. I. Nandasiri, S. Kuchibhatla, L. Kovarik, S. Thevuthasan and S. Prasad, *Solid State Ionics*, 2011, **204-205**, 13–19.
[8] M. G. Bellino, D. G. Lamas and Walsöe de Reca, N. E., *Advanced Functional Materials*, 2006, **16**, 107–113.
[9] S. Omar, E. D. Wachsman, J. L. Jones and J. C. Nino, *Journal of the American Ceramic Society*, 2009, **92**, 2674–2681.
[10] D. Pérez-Coll, D. Marrero-López, P. Núñez, S. Piñol and J. R. Frade, *Electrochimica Acta*, 2006, **51**, 6463–6469.
[11] J. van Herle, D. Seneviratne and A. McEvoy, *Journal of the European Ceramic Society*, 1999, **19**, 837–841.
[12] J. Van herle, T. Horita, T. Kawada, N. Sakai, H. Yokokawa and M. Dokiya, *Solid State Ionics*, 1996, **86-88**, 1255–1258.
[13] Y. Zheng, M. Zhou, L. Ge, S. Li, H. Chen and L. Guo, *Journal of Alloys and Compounds*, 2011, **509**, 1244–1248.
[14] W. Zajac, *Solid State Ionics*, 2008, **179**, 154–158.
[15] B. Steele, *Solid State Ionics*, 2000, **129**, 95–110.
[16] Z. Tianshu, P. Hing, H. Huang and J. Kilner, *Solid State Ionics*, 2002, **148**, 567–573.
[17] B. Steele, K. Zheng, R. Rudkin, N. Kiratzis and M. Cristie, in *Proceedings of the Fourth International Symposium on Solid Oxide Fuel Cells (SOFC-IV)*, ed. M. Dokiya, Electrochemical Society, Pennington, NJ, 1995, vol. 95-1 of Proceedings of the Electrochemical Society, pp. 1028–1038.
[18] K. Huang, M. Feng and J. B. Goodenough, *Journal of the American Ceramic Society*, 1998, **81**, 357–362.
[19] E. Ruiz-Trejo, J. D. Sirman, Y. M. Baikov and J. A. Kilner, *Solid State Ionics*, 1998, **113-115**, 565–569.
[20] G. Christie, *Solid State Ionics*, 1996, **83**, 17–27.
[21] K. R. Reddy and K. Karan, *Journal of Electroceramics*, 2005, **15**, 45–56.
[22] J. Koettgen and M. Martin, *Journal of the American Ceramic Society*, 2020, **103**, 3776–3787.
[23] S. Grieshammer, S. Eisele and J. Koettgen, *The Journal of Physical Chemistry C*, 2018, **122**, 18809–18817.
[24] A. Trovarelli, *Catalysis Reviews*, 1996, **38**, 439–520.
[25] M. Nolan, V. S. Verdugo and H. Metiu, *Surface Science*, 2008, **602**, 2734–2742.
[26] F. Call, M. Roeb, M. Schmücker, H. Bru, D. Curulla-Ferre, C. Sattler and R. Pitz-Paal, *American Journal of Analytical Chemistry*, 2013, **04**, 37–45.
[27] Y. Hao, C.-K. Yang and S. M. Haile, *Chemistry of Materials*, 2014, **26**, 6073–6082.
[28] F. Call, M. Roeb, M. Schmücker, C. Sattler and R. Pitz-Paal, *The Journal of Physical Chemistry C*, 2015, **119**, 6929–6938.
[29] J. Koettgen, T. Zacherle, S. Grieshammer and M. Martin, *Physical Chemistry Chemical Physics*, 2017, **19**, 9957–9973.
[30] J.-P. Eufinger, M. Daniels, K. Schmale, S. Berendts, G. Ulbrich, M. Lerch, H.-D. Wiemhöfer and J. Janek, *Physical Chemistry Chemical Physics*, 2014, **16**, 25583–25600.
[31] J. Koettgen and M. Martin, *Solid State Communications*, 2020, **314-315**, 113939.
[32] D. Andersson, S. Simak, N. Skorodumova, I. Abrikosov and B. Johansson, *Physical Review B*, 2007, **76**, 174119.
[33] D. A. Andersson, S. I. Simak, N. V. Skorodumova, I. A. Abrikosov and B. Johansson, *Applied Physics Letters*, 2007, **90**, 031909.
[34] H.-T. Chen and J.-G. Chang, *The Journal of Chemical Physics*, 2010, **132**, 214702.
[35] Y. Tang, H. Zhang, L. Cui, C. Ouyang, S. Shi, W. Tang, H. Li, J.-S. Lee and L. Chen, *Physical Review B*, 2010, **82**, 125104.
[36] G. Ulbrich, *Ph.D. Thesis*, Technische Universität Berlin, Berlin, 2015.
[37] J. Koettgen and M. Martin, *The Journal of Physical Chemistry C*, 2019, **123**, 6333–6339.

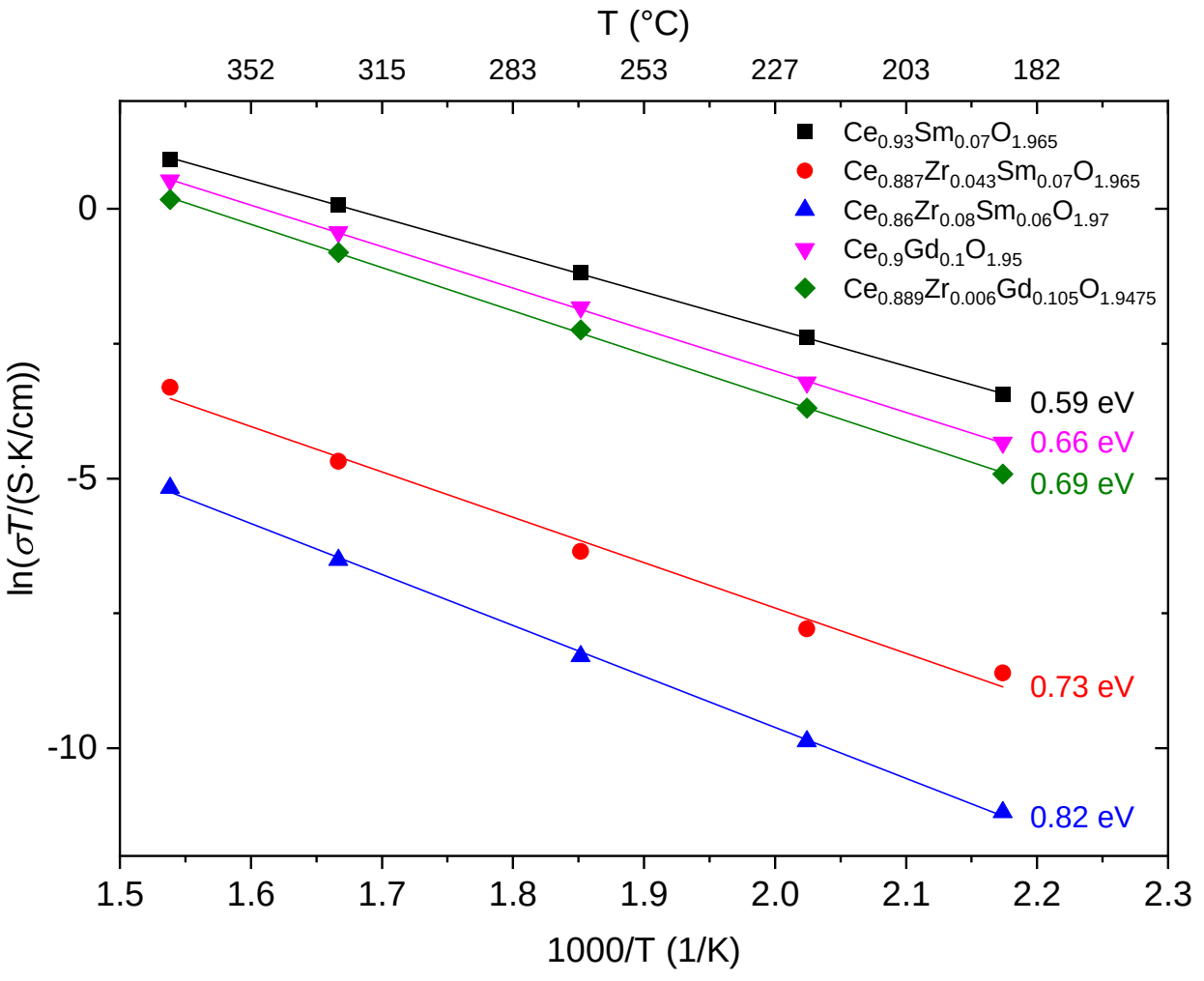

Figure 6: Ionic conductivity of Sm-Zr and Gd-Zr doped ceria according to Kinetic Monte Carlo Simulations.

[38] T. Leichtweiss, R. A. Henning, J. Koettgen, R. M. Schmidt, B. Holländer, M. Martin, M. Wuttig and J. Janek, *Journal of Materials Chemistry A*, 2014, **2**, 6631.
[39] D. Y. Wang and A. S. Nowick, *Journal of Solid State Chemistry*, 1980, **35**, 325–333.
[40] J. Koettgen, P. C. Schmidt, T. Bučko and M. Martin, *Physical Review B*, 2018, **97**, 024305.
[41] J. Koettgen and M. Martin, *The Journal of Physical Chemistry C*, 2019, **123**, 19437–19446.
[42] G. Kresse and J. Furthmüller, *Physical Review B*, 1996, **54**, 11169–11186.
[43] G. Kresse and D. Joubert, *Physical Review B*, 1999, **59**, 1758–1775.
[44] J. P. Perdew, K. Burke and M. Ernzerhof, *Physical Review Letters*, 1997, **78**, 1396.
[45] J. Hafner, *Journal of Computational Chemistry*, 2008, **29**, 2044–2078.
[46] P. E. Blöchl, *Physical Review B*, 1994, **50**, 17953–17979.
[47] S. L. Dudarev, G. A. Botton, S. Y. Savrasov, C. J. Humphreys and A. P. Sutton, *Physical Review B*, 1998, **57**, 1505–1509.
[48] M. Nolan and J. E. W. G. W. Fearon, *Solid State Ionics*, 2006, **177**, 3069–3074.
[49] Z. Yang, G. Luo, Z. Lu and K. Hermansson, *The Journal of Chemical Physics*, 2007, **127**, 074704.
[50] Z. Yang, G. Luo, Z. Lu, T. K. Woo and K. Hermansson, *Journal of Physics: Condensed Matter*, 2008, **20**, 035210.
[51] J. Hooper, A. Ismail, J. B. Giorgi and T. K. Woo, *Physical Chemistry Chemical Physics*, 2010, **12**, 12969.
[52] P. P. Dholabhai, J. B. Adams, P. Crozier and R. Sharma, *Physical Chemistry Chemical Physics*, 2010, **12**, 7904.
[53] P. P. Dholabhai, J. B. Adams, P. Crozier and R. Sharma, *The Journal of Chemical Physics*, 2010, **132**, 094104.
[54] A. Ismail, J. Hooper, J. B. Giorgi and T. K. Woo, *Physical Chemistry Chemical Physics*, 2011, **13**, 6116.
[55] P. P. Dholabhai and J. B. Adams, *Journal of Materials Science*, 2012, **47**, 7530–7541.
[56] T. Zacherle, P. C. Schmidt and M. Martin, *Physical Review B*, 2013, **87**, 235206.
[57] J. X. Zheng, G. Ceder, T. Maxisch, W. K. Chim and W. K. Choi, *Physical Review B*, 2006, **73**, 104101.

[58] J. Wang, Y. Du, H. Xu, C. Jiang, Y. Kong, L. Sun and Z.-K. Liu, *Physical Review B*, 2011, **84**, 024107.
[59] X. Li, M. W. Finnis, J. He, R. K. Behera, S. R. Phillpot, S. B. Sinnott and E. C. Dickey, *Acta Materialia*, 2009, **57**, 5882–5891.
[60] F. D. Murnaghan, *American Journal of Mathematics*, 1937, **59**, 235.
[61] F. D. Murnaghan, *Proceedings of the National Academy of Sciences*, 1944, **30**, 244–247.
[62] F. Birch, *Physical Review*, 1947, **71**, 809–824.
[63] J. L. F. Da Silva, M. V. Ganduglia-Pirovano, J. Sauer, V. Bayer and G. Kresse, *Physical Review B*, 2007, **75**, 045121.
[64] P. R. L. Keating, D. O. Scanlon, B. J. Morgan, N. M. Galea and G. W. Watson, *The Journal of Physical Chemistry C*, 2012, **116**, 2443–2452.
[65] T. Zacherle, A. Schriever, R. A. De Souza and M. Martin, *Physical Review B*, 2013, **87**, 134104.
[66] G. Mills, H. Jónsson and G. K. Schenter, *Surface Science*, 1995, **324**, 305–337.
[67] H. Jonsson, G. Mills and K. M. Jacobsen, in *Classical and quantum dynamics in condensed phase simulations*, ed. B. J. Berne, World Scientific, Singapore, 1998, pp. 385–404.
[68] M. Lumeij, J. Koettgen, M. Gilleßen, T. Itoh and R. Dronskowski, *Solid State Ionics*, 2012, **222-223**, 53–58.
[69] G. Henkelman, B. P. Uberuaga and H. Jónsson, *The Journal of Chemical Physics*, 2000, **113**, 9901.
[70] G. Makov and M. C. Payne, *Physical Review B*, 1995, **51**, 4014–4022.
[71] P. P. Dholabhai, J. B. Adams, P. A. Crozier and R. Sharma, *Journal of Materials Chemistry*, 2011, **21**, 18991.
[72] P. Hein, B. O. H. Grope, J. Koettgen, S. Grieshammer and M. Martin, *iCon: A general lattice Kinetic Monte Carlo program*, 2020.
[73] D. K. Hohnke, *Solid State Ionics*, 1981, **5**, 531–534.
[74] M. Martin, *Journal of Electroceramics*, 2006, **17**, 765–773.
[75] A. Murray, G. Murch and C. Catlow, *Solid State Ionics*, 1986, **18-19**, 196–202.
[76] S. B. Adler and J. W. Smith, *Journal of the Chemical Society, Faraday Transactions*, 1993, **89**, 3123.
[77] M. Meyer and N. Nicoloso, *Berichte der Bunsen-Gesellschaft*, 1997, **101**, 1393–1398.
[78] A. Oaks, Di Yun, B. Ye, W.-Y. Chen and J. F. Stubbins, *Journal of Nuclear Materials*, 2011, **414**, 145–149.
[79] P. P. Dholabhai, S. Anwar, J. B. Adams, P. Crozier and R. Sharma, *Journal of Solid State Chemistry*, 2011, **184**, 811–817.
[80] P. P. Dholabhai, S. Anwar, J. B. Adams, P. A. Crozier and R. Sharma, *Modelling and Simulation in Materials Science and Engineering*, 2012, **20**, 015004.
[81] J. O. Nilsson, M. Leetmaa, O. Y. Vekilova, S. I. Simak and N. V. Skorodumova, *Physical Chemistry Chemical Physics*, 2017, **19**, 13723–13730.
[82] B. O. H. Grope, T. Zacherle, M. Nakayama and M. Martin, *Solid State Ionics*, 2012, **225**, 476–483.
[83] D. Wang, D. Park, J. Griffith and A. Nowick, *Solid State Ionics*, 1981, **2**, 95–105.
[84] T. Zhang, J. Ma, L. Kong, S. Chan and J. Kilner, *Solid State Ionics*, 2004, **170**, 209–217.
[85] D. Pérez-Coll, P. Núñez and J. R. Frade, *Journal of The Electrochemical Society*, 2006, **153**, A478.
[86] I. Stephens and J. Kilner, *Solid State Ionics*, 2006, **177**, 669–676.
[87] S. Haile, G. Staneff and K. Ryu, *Journal of Materials Science*, 2001, **36**, 1149–1160.
[88] E. Chinarro, *Solid State Ionics*, 2003, **160**, 161–168.
[89] J. Bauerle, *Journal of Physics and Chemistry of Solids*, 1969, **30**, 2657–2670.
[90] J. R. Köttgen, *PhD thesis*, RWTH Aachen University, 2017.
[91] S. Grieshammer, *Phys. Chem. Chem. Phys.*, 2018, **20**, 19792–19799.
[92] Jülich Supercomputing Centre, *Journal of large-scale research facilities*, 2016, **2**, A62.